Journal of Molecular Catalysis A: Chemical 310 (2009) 17–23

Contents lists available at ScienceDirect

Journal of Molecular Catalysis A: Chemical

journal homepage: www.elsevier.com/locate/molcata

Bulk and surface structures of V_2O_5/ZrO_2 catalysts for *n*-butane oxidative dehydrogenation

Delia Gazzoli [a,*], Sergio De Rossi [b], Giovanni Ferraris [b], Giorgio Mattei [c,1], Roberto Spinicci [d], Mario Valigi [a]

[a] *Dipartimento di Chimica, Sapienza Università di Roma, P.le A. Moro, 5, I-00185 Rome, Italy*
[b] *Consiglio Nazionale delle Ricerche, Istituto dei Sistemi Complessi, ISC, UOS "Materiali Inorganici e Catalisi Eterogenea" (MICE), c/o Dipartimento di Chimica, Sapienza Università di Roma, P.le A. Moro, 5, I-00185 Rome, Italy*
[c] *Consiglio Nazionale delle Ricerche, Istituto dei Sistemi Complessi, ISC, Sezione di Montelibretti (Roma) - Via Salaria Km 29.300, C.P. 10, I-00016 Monterotondo St., Italy*
[d] *Dipartimento di Energetica, Università di Firenze, via S. Marta, 3, I-50139 Florence, Italy*

ARTICLE INFO

Article history:
Received 1 December 2008
Received in revised form 14 May 2009
Accepted 17 May 2009
Available online 27 May 2009

Keywords:
Butane ODH
V_2O_5/ZrO_2
Zirconia
Raman spectroscopy
TPR

ABSTRACT

The present investigation focuses on the structural properties and reactivity of zirconia-supported vanadium oxide catalysts, prepared by equilibrium adsorption in basic (pH 10) or in acid (pH 2.7) conditions with vanadium content up to 6 wt.% (pH 10) and up to 11.6 wt.% (pH 2.7). The samples, heated at 823 K for 5 h in air, were characterized by X-ray diffraction, Raman spectroscopy and TPR, both as prepared and after leaching with an ammonia solution to remove species not anchored to the zirconia surface. Some representative samples were also tested for the *n*-butane oxidative dehydrogenation (ODH) reaction. Depending on vanadium content, various vanadium species were identified by Raman spectroscopy that reacted differently on exposure to H_2. At similar loading, the fraction of vanadium in a dispersed state and thus interacting with the support was higher in samples prepared at pH 10 than in those at pH 2.7. Samples prepared at pH 2.7 contained a higher fraction of large polymeric structures in addition to ZrV_2O_7 and V_2O_5.

In line with literature data for propane ODH on similar catalysts, our catalytic results suggested that the active sites for the ODH reaction are associated with the V–O–V bonds of the polymeric exposed structures, whereas the Zr–O–V sites favour alkane combustion.

1. Introduction

Vanadium oxides supported on various metal oxides (e.g., MgO, TiO_2, Al_2O_3, ZrO_2, SiO_2) are an important group of catalysts for a variety of reactions, including selective oxidation of hydrocarbons [1–6], ammoxidation of aromatics and alkyl-aromatics [7] and selective catalytic reduction of NO with NH_3 [8,9]. Their surface properties have been analyzed in detail and many studies have investigated the relationship between their surface structure and catalytic properties [6,10–15]. In particular, ZrO_2 supported vanadium oxide samples have been investigated as catalysts for the oxidative dehydrogenation (ODH) reaction of alkanes, one of the most feasible processes to obtain light olefins [16–18]. Numerous studies have focused on propane ODH [19–24]. The vanadium dispersed species have been extensively characterized by various techniques and related to the catalytic activity and selectivity in propane ODH [19,20]. Other studies have reported detailed ODH kinetics, including activation energies and entropies for primary and secondary combustion [22–24]. Conversely, although ample information is available on the ODH reaction of *n*-butane on several catalysts [25,26], to our knowledge little is known about the same reaction on VO_x/ZrO_2 catalysts. As the reactivity of *n*-butane on various vanadium based catalysts is higher than that of propane [2,27,28], we thought interesting to explore the behaviour of VO_x/ZrO_2 catalysts in the ODH reaction of *n*-butane to butenes. As a practical aspect, butenes reacting with isobutane yield high octane number branched C_8 alkanes for gasoline reformulation.

The efficiency of supported vanadium oxide catalysts mainly depends on the dispersion of the active phase, which in turn depends closely on the supported oxide and the method used for catalyst preparation. In a previous investigation of the zirconia-supported vanadium oxide systems, we found that the uptake of vanadium species on the hydrous support, obtained by equilibrium adsorption at pH 10 or at pH 2.7, depended on the preparation pH [29]. After heating at 823 K, for catalysts having similar vanadium loading the fraction of vanadium in a dispersed state and interacting with the support was higher in samples at pH 10 than in those prepared at pH 2.7. Compared to samples prepared at pH 10, those at pH 2.7 contained a higher fraction of vanadium as ZrV_2O_7 and V_2O_5.

* Corresponding author. Tel.: +39 06 49913377; fax: +39 06 490324.
E-mail address: delia.gazzoli@uniroma1.it (D. Gazzoli).
[1] Deceased.

1381-1169/$ – see front matter © 2009 Elsevier B.V. All rights reserved.
doi:10.1016/j.molcata.2009.05.014

Table 1
Specific surface area, S, and crystalline phases for vanadium-supported zirconia samples as prepared (heated at 823 K, for 5 h, in air) and after leaching with an ammonia solution.

Samples[a]	S($m^2\ g^{-1}$)	Phases[b]	Samples[a]	S($m^2\ g^{-1}$)	Phases[b]
ZrO_2(823)	49	m, t			
ZV0.99,10	79	m, t	ZV 1.2,2.7	60	m, t
ZV2.7,10	77	m, t	ZV 1.9,2.7	77	m, t
ZV3.1,10	105	m, t	ZV 2.6,2.7	97	m, t
ZV3.4,10	128	m, t	ZV3.7,2.7	80	m, t
ZV4.1,10	116	m, t	ZV 5.3,2.7	42	m, t, Z, V
ZV4.2,10	96	m, t	ZV 5.9,2.7	37	m, t, Z, V
ZV4.8,10	86	m, t	ZV 7.4,2.7	24	m, t, Z, V
ZV5.4,10	100	m, t	ZV 7.6,2.7	38	m, t, Z, V
ZV6.4,10	114	m, t	ZV 11.6,2.7	39	m, t, Z, V
ZV2.710L1.4	77	m, t	ZV1.2,2.7L1.1	60	m, t
ZV2.8,10 L1.8	100	m, t	ZV1.9,2.7L1.0	77	m, t
ZV3.4,10L2.5	128	m, t	ZV5.3,2.7L2.0	45	m, t, Z
ZV4.1,10L2.2	116	m, t	ZV 5.9,2.7L2.3	42	m, t, Z
ZV4.8,10L2.2	89	m, t	ZV7.4,2.7L5.8	35	m, t, Z
ZV5.4,10L3.0	102	m, t,	ZV7.6,2.7L5.7	45	m, t, Z

[a] For designation of samples, see text.
[b] m = monoclinic ZrO_2; t = tetragonal ZrO_2, Z = ZrV_2O_7; V = V_2O_5.

In both series of samples vanadium invariably tended to condense into polymeric species resulting in a multilayer material.

In this study, we have examined the two series of samples in greater detail and tested their catalytic behaviour for the ODH reaction of *n*-butane. To differentiate the catalytic activity of the various vanadium species on the zirconia surface or reacted with the support, the samples were studied as prepared and after leaching with an ammonia solution. The leaching treatment has already been applied to vanadium-supported catalysts [30–32].

For the study we used several techniques including X-ray diffraction, Raman spectroscopy, temperature-programmed reduction determinations and catalytic tests.

2. Experimental

2.1. Sample preparation

The samples were prepared as previously described [29]. Hydrous zirconium oxide was precipitated by bubbling a stream of ammonia-saturated N_2 into a $ZrOCl_2$ solution for 18 h [33]. After separation the solid was washed (Cl^- negative test in the solid), and dried at 383 K, 24 h. The obtained hydrous zirconium oxide was microporous, (specific surface area: 330 $m^2\ g^{-1}$) and amorphous to X-ray. It was designated as ZrO_2(383). The vanadium containing samples were obtained by equilibrium adsorption suspending ZrO_2(383) in V(V) aqueous solutions (from NH_4VO_3, Fluka) at pH 10 or 2.7 (fixed by NH_4OH or HNO_3). The suspension was shaken for 72 h at room temperature to equilibrate the system. The solid was filtered from the liquid fraction, dried at 383 K for 24 h and finally heated in air at 823 K, 5 h. A fraction of ZrO_2(383), contacted with water, underwent similar treatment (shaking, filtering, heating at 823 K, 5 h) and was indicated as ZrO_2(823). The samples containing vanadium were designated as ZV*x*,*y*, where *x* stands for the vanadium content as wt.% (metal) and *y* the pH value (Table 1). Some samples were leached with a hot ammonia solution (about 20 mL, 2 mol L^{-1}) in a closed vessel for 30 min, under stirring to eliminate soluble vanadium. The solid was then separated and the leaching repeated three times. The liquid fractions were collected and used to determine the soluble vanadium content. The leached samples were indicated as ZV*x*,*y*L*z*, where *x* and *y* as stated, L stands for leaching and *z* for the vanadium content remaining in the sample (wt.%).

V_2O_5 was obtained by decomposing NH_4VO_3 (Fluka) in air at 873 K for 3 h. ZrV_2O_7 was prepared heating a mixture of V_2O_5 and ZrO_2(383) in air at 983 K, following the procedure described by Sanati et al. [34]. Because at 983 K some V_2O_5 becomes volatile, a small excess of V_2O_5, compared with the stoichiometric ratio, was added to the reacting mixture. The pentoxide in excess was removed by leaching with an ammonia solution [35]. After rinsing the solid was re-heated at 773 K 1 h in air. The X-ray diffraction patterns of the prepared V_2O_5 and ZrV_2O_7 corresponded to those reported in the JCPDS diffraction files [36,37]. The crystallite-size, *D*, determined from the line broadening of the most intense reflexions of V_2O_5 and ZrV_2O_7 resulted $D_{V_2O_5} = 75$ nm and $D_{ZrV_2O_7} > 200$ nm. In the most concentrated ZV*x*,2.7, the crystallite-size of ZrV_2O_7 was about 100 nm.

2.2. Experimental techniques

The vanadium content was determined by atomic absorption after dissolution of the sample in a concentrated HF solution, and subsequent dilution [38]. The standard solution (Fluka 1000 ppm) contained ZrO_2, dissolved in HF, in a concentration similar to that of the samples.

X-ray diffraction (XRD) patterns in the 2θ angular range from 5° to 60° were obtained with a Philips PW 1729 diffractometer using Cu Kα (Ni-filtered) radiation.

Surface areas were determined by N_2 adsorption at 77 K (BET method) using a Micromeritics apparatus ASAP 2010.

Raman spectra were collected with a SPECS triple spectrograph, in macro configuration, equipped with a liquid-nitrogen-cooled CCD detector using the 514.5 nm line of an Ar^+ laser. The laser power on the sample was always kept under 20 mW. The polarization of the scattered light was not analyzed. The spectral resolution was 1.4 cm^{-1}. The samples were pressed into 5 mm pellets and analyzed in air or using a *in situ* cell. Details of the cell setup are given elsewhere [39]. In the *in situ* experiment, the sample was heated in flowing dry oxygen at 673 K, 2 h and the spectra were collected after cooling to 298 K always in dry oxygen. Raman spectra analysis included smoothing, base line removal and curve fitting by a GRAMS/386 software by Galactic.

Temperature-programmed reduction (TPR) was measured/analyzed in a flow system using a HWD detector and a gas mixture containing 10 vol.% of hydrogen in nitrogen 1.8 dm^3/h, heating rate 8 K/min. The gases were dried and purified with suitable filters and their flows regulated with Brooks electronic mass flow controllers. For the measurement, 60 mg of sample, located in a tubular reactor, underwent oxidative pre-treatment in a flow of oxygen (20 vol.%) in nitrogen at 723 K, 1 h, cooled to room temperature in a nitrogen flow and then equilibrated in the reaction mixture.

The *n*-butane ODH reaction was studied at ambient pressure in a tubular continuous flow microreactor containing 90 mg of powdered sample. The gases were purified and dehydrated by means of suitable filters and their flows were regulated by means of MKS electronic mass flow controllers. Before the test, the catalyst was pre-treated *in situ* in a flow of oxygen (20 mol%) in helium at 723 K, 1 h, and cooled to reaction temperature in a helium flow. The experiments were conducted at 603 K with a reactant mixture containing 2.7 mol% *n*-C_4H_{10}, 4.1 mol% O_2, balance He, at total flow rate of 73 ml min^{-1}. In preliminary experiments, some samples were tested with different gas feed mixtures (O_2/*n*-butane ratio 1, 2, 4) and at 563 K and 643 K. At constant temperature, the increase of the reactant O_2 invariably brought about a little increase in the *n*-butane total conversion and a moderate decrease in the butene selectivity. At constant gas feed mixture (O_2/*n*-butane ratio) the increase of the reaction temperature, apart from the obvious increase of the total conversion, reduced the butene selectivity.

Because the results were not unexpected and did not add much information, they were not reported and for all catalysts we chose to operate at the condition reported above. Gas analysis was done with a PerkinElmer Autosystem gas chromatograph, equipped with Plot-Q capillary columns and HWD detector. The % butane total conversion, $\%C_{tot}$, and the % selectivity to butenes, $\%S_{butenes}$, were calculated as:

$$\%C_{tot} = 100\frac{(C_4H_{10})_{in} - (C_4H_{10})_{out}}{(C_4H_{10})_{in}}$$

$$\%S_{butenes} = 100\frac{(C_4H_8)_{out}}{(C_4H_{10})_{in} - (C_4H_{10})_{out}}$$

The areal rates of total n-C_4H_{10} conversion (r_{tot}) were calculated as the number of molecules converted *per* second and *per* nm^2 of sample exposed area. All reported catalysis data were collected at the steady state. Owing to the mesoporous character of the materials [29], we did not expect rate limitation due to mass transfer within the pores, as they are quite larger than the involved molecules.

3. Results and discussion

3.1. Catalyst characterization

For all ZV*x*,*y* samples the specific surface area values were higher than that of ZrO_2(823), increasing for vanadium content up to $x \sim 3$ wt.% (Table 1). For higher vanadium content, the specific surface area values of the ZV*x*,10 samples remained practically constant, whereas those of the ZV*x*,2.7 set markedly decreased. Leaching with ammonia solution did not affect significantly the surface area values.

The X-ray diffraction analysis of samples ZV*x*,10 revealed no lines other than those of ZrO_2, both in the monoclinic and tetragonal modification (Fig. 1A). Nor did the ZV*x*,2.7 samples with $x \leq 3.7$ wt.%, but for samples with higher vanadium concentration the lines of ZrV_2O_7 and V_2O_5 were also detected (Fig. 1B). The V_2O_5 reflections were no longer present in the patterns of leached samples. The intensity of the tetragonal peaks increased relative to that of monoclinic peaks with increasing vanadium loading in both series of samples (Fig. 1). The comparison of the X-ray patterns of ZV2.7,10 and ZV2.6,2.7 samples (Fig. 1A, curve a and Fig. 1B, curve b reveals that, despite the almost equal concentration, the fraction of tetragonal zirconia in the ZV2.7,10 is higher than in ZV2.6,2.7.

All these findings are in agreement with the results reported in a previous paper [29], where we showed that, owing to the prevailing microporous texture of ZrO_2(383) and the influence of pH on the size of vanadium species, after heating at 823 K the two sets of samples differed in the fraction of the various vanadium species. The interaction of vanadium species with the zirconia surface affected some solid state processes of the support, including phase transition and sintering, an effect well documented for various systems composed of transition metal oxoanions supported on zirconia [19,29,40,41].

Raman spectroscopy has been used to determine the structure of the vanadium species both in amorphous and crystalline form. Raman spectra recorded for ZV*x*,10 (Fig. 2A) and ZV*x*,2.7 (Fig. 2B), under ambient conditions, exhibited bands in the range 200–700 cm^{-1} due to ZrO_2 (monoclinic and tetragonal) and a composite feature spanning the frequencies range 750–1040 cm^{-1} due to vanadium species. At increasing vanadium content the bands of ZrO_2 progressively diminished in intensity and for $x > 5$ wt.% they were barely detectable in both series of samples, indicating that the thickness of the vanadium species on the zirconia surface increased.

All ZV*x*,10 samples (Fig. 2A) and ZV*x*, 2.7 with vanadium content lower than 5.3 wt.% (Fig. 2B, curves a and b) showed similar spectra, characterized by a broad feature centred at about 885 cm^{-1} corresponding to V–O–V vibrations and bands in the range 1000–1030 cm^{-1} depending on V content assigned to V=O vibrations of VO_x species in polyvanadate structures [21,23,42–45].

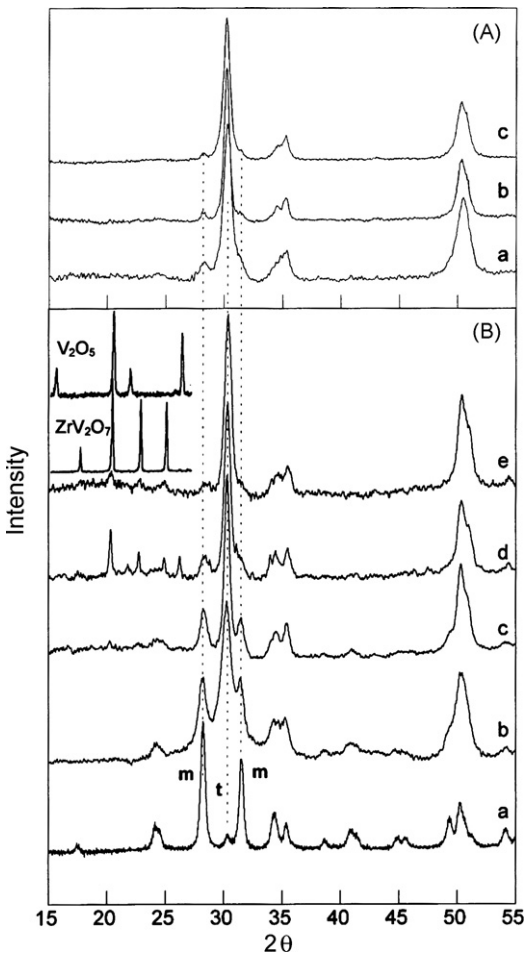

Fig. 1. XRD spectra for ZV*x*,10 (A) and ZV*x*,2.7 (B) samples. Section A: (a) ZV2.7,10; (b) ZV4.2,10; (c) ZV6.4,10. Section B: (a) ZrO_2(823); (b) ZV2.6,2.7; (c) ZV5.3,2.7; (d) ZV11.6,2.7; (e) ZV11.6,2.7L6. Dotted lines indicate the most intense reflections of monoclinic, m, and tetragonal, t, zirconia.

In the spectra of ZV*x*,2.7 samples with $x \geq 5.3$ wt.% bands at 775 cm^{-1} and 989 cm^{-1} (Fig. 2B, curves c–e) due to ZrV_2O_7 (Fig. 2B, curve f) [20], were also clearly detected; their intensities increased with the vanadium content. The spectrum of the concentrated ZV7.6,2.7 sample (Fig. 2B, curve e) showed, in addition, sharp bands at about 142 cm^{-1} and 998 cm^{-1}, identifying the presence of V_2O_5 (Fig. 2B, curve g) [46]. The Raman assignment is consistent with XRD results (Fig. 1) indicating that, besides vanadium polymeric species, the concentrated ZV*x*,2.7 samples contained ZrV_2O_7 or V_2O_5 or both.

A deeper insight on the molecular structure of the surface species and on the interaction between vanadium species and the support is achieved by the analysis of the Raman spectra collected under dehydrated conditions ("*in situ*" treatment at 673 K, 2 h in flowing dry oxygen). It is well documented that hydration affects vanadium surface species probably via hydrogen bonding resulting in a shift to lower frequencies and broadening of the terminal V=O band [47]. Compared to the spectra under ambient condition, those collected in dry conditions showed a modification in the range 1000–1030 cm^{-1}, but not in the region 750–950 cm^{-1}. Raman spectra under dry conditions of some representative ZV*x*,10 (Fig. 3A and B) and ZV*x*,2.7 (Fig. 3C and D) samples are presented

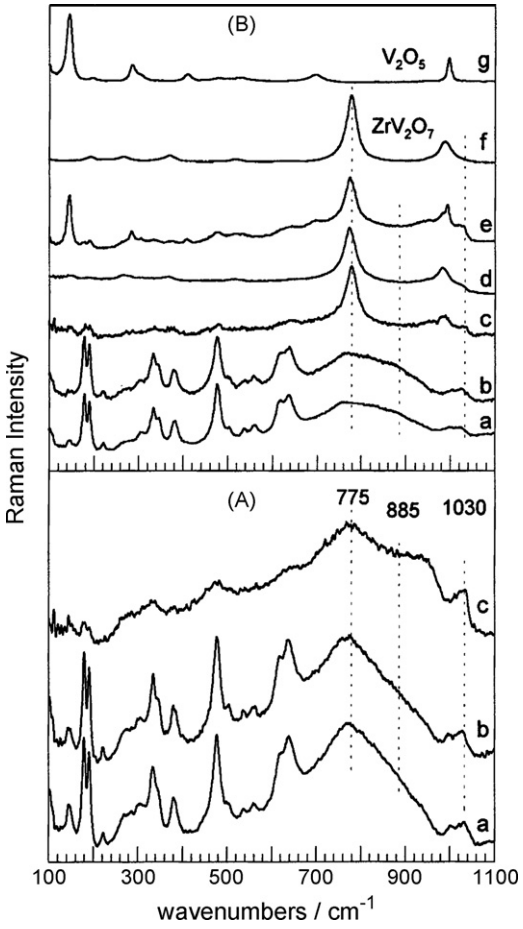

Fig. 2. Raman spectra of ZV*x*,10 (A) and ZV*x*,2.7 (B) samples. Section A: (a) ZV2.7,10; (b) ZV4.8,10; (c) ZV5.4,10. Section B: (a) ZV1.2,2.7; (b) ZV1.9,2.7; (c) ZV5.3,2.7; (d) ZV7.4,2.7; (e) ZV7.6,2.7; (f) ZrV_2O_7; (g) V_2O_5.

together with those of samples after ammonia leaching. Bands at about 1000 cm^{-1} and 1025 cm^{-1} were observed in the ZV2.7,10 sample (Fig. 3A, curve a) and at about 1017 cm^{-1} and 1033 cm^{-1} in the ZV5.4,10 sample (Fig. 3B, curve a). For the ZV*x*,2.7 samples, low intensity bands at about 1000 cm^{-1} and 1025 cm^{-1} were detected in the spectrum of the diluted ZV1.2,2.7 sample (Fig. 3C, curve a), whereas in the concentrated ZV7.4,2.7 sample only the band at about 1033 cm^{-1} (Fig. 3D, curve a) was clearly seen, because the one at about 1000 cm^{-1} was obscured by the intense band at about 985 cm^{-1} due to ZrV_2O_7 (Fig. 3D, curve a). The shift to higher frequencies of the bands in the 1000–1030 cm^{-1} range and the concomitant growing in intensity of the broad feature in the 750–950 cm^{-1} region at increasing vanadium content indicate the presence of polyvanadate structures that increase in size or number or both with vanadium loading.

The inspection of the Raman spectra collected on leached samples (Fig. 3A–D, curves b) specifies that the leaching caused several effects: removed the bands at $\nu > 1020\ cm^{-1}$ (V=O) (inset of Fig. 3A–D), lowered the intensity of the broad feature in the region 750–950 cm^{-1} (Fig. 3A–D) and disclosed the bands at about 775 and 985cm^{-1} already at low vanadium content (Fig. 3A–D). From these findings, more pronounced at increasing vanadium content, we infer that the leaching removes some large polymeric vanadates and V_2O_5 when present, leaving on the support surface small sized polymeric structures and ZrV2O7. The band at about 1010 cm^{-1} in the ZV1.2,2.7L1.1 sample, could indicate monovanadates species (V=O stretching mode) [44], whereas the coexistence of the broad feature at about 850 cm^{-1}, suggests V–O–V modes within polyvanadates structures (Fig. 3C, curve a), although the occurrence of isolated monovanadates species cannot be disregarded.

Changes in the surface morphology of zirconia-supported vanadium oxide systems with ammonia leaching imaged by atomic force microscopy (TM-AFM) strengthen the view that large polymeric vanadium material grows over vanadium species interacting with zirconia [48]. In samples prepared by ionic exchange between an aqueous solution of peroxovanadate complexes and hydrous zirconium oxide (V content up to 6.8 wt.%) and heated in air at 823 K for 5 h as for the present systems [48], AFM revealed that, as vanadium content increased, the surface morphology evolved from a smooth surface profile towards a granular surface (roundish particles about 90–100 nm in diameter and about 20–30 nm in height) with some larger grains, grown layered, with a lateral size of 200–250 nm and 35–40 nm in height. Leaching produced an overall flattening of the system: the large structures (250–300 nm) were almost completely removed, the roundish structures were left unchanged in size and some aggregates became more clearly visible.

TPR analysis of our samples confirmed the presence of various vanadium species. TPR data may strongly depend on the experimental conditions and, although the information obtained is merely comparative [49], this technique may help to characterize the reducibility of different species [50]. ZrO_2 showed no reduction processes in the temperature range investigated (not shown). The TPR profile of V_2O_5 (not shown) consisted of several peaks in the temperature range 920–1130 K in agreement with literature data [49–52]. The profile for ZrV_2O_7 displayed a narrow peak at about 813 K and a low-intensity tail in the range 573–773 K (Fig. 4B, curve g). We note that a TPR profile of ZrV_2O_7 was already reported by Pieck et al. [51] with three peaks appearing at 700 K, 823 K and 860 K. The two peaks at 700 K and 823 K were probably related to the reduction of vanadium surface species that are soluble in ammonia solution and thus are absent in TPR profile of our sample. Three features could be identified from the complex TPR profiles of the ZV*x*,10 samples: a main component at about 713 K and H_2 uptakes at lower (523–623 K) and higher (773–923 K) temperatures (Fig. 4A). At increasing vanadium content, the main peak increased in intensity and became asymmetric toward the high temperature side. For the ZV5.4,10 sample distinct H_2 consumption was detected at 753 K (Fig. 4A, curve f). The reducibility of the diluted ZV*x*,2.7 samples (Fig. 4B, curves a and b) almost matched that of samples prepared at pH 10 confirming the presence of species of similar typology. At increasing vanadium content the main hydrogen consumption shifted to the range 770–820 K (Fig. 4B, curves c–f), partially overlapping the temperature range at which ZrV_2O_7 reduces (Fig. 4B, curve g) and, the more concentrated sample showed a distinct peak at about 900 K, due to V_2O_5 (Fig. 4B, curve f), in agreement with X-ray analysis. We assign the hydrogen consumption in the range 580–620 K to small polymeric VO_x anchored to the zirconia surface and in the range 680–730 K to larger polymeric aggregates. The reduction in the range 770–820 K identified ZrV_2O_7.

The reducibility of vanadium species interacting with different supports has already been investigated [52,53]. Studying the vanadia/alumina and vanadia/zirconia systems, Roozeboom et al. [52] observed two reduction peaks, depending on vanadium content: at low vanadium content (<2.5 wt.%) the peak occurred in the range 650–700 K, whereas for more concentrated samples the peak was centred at about 600 K. For vanadia/zirconia samples, Adamski et al. [53] found a TPR peak at about 800 K at low vanadium content ascribed to monovanadates; at increasing concentration the TPR profile first shifted to lower temperatures (formation of small polymers) and then (formation of large polymeric species, V_2O_5-like) moved back towards the reduction temperature observed for V_2O_5. These investigators observed that

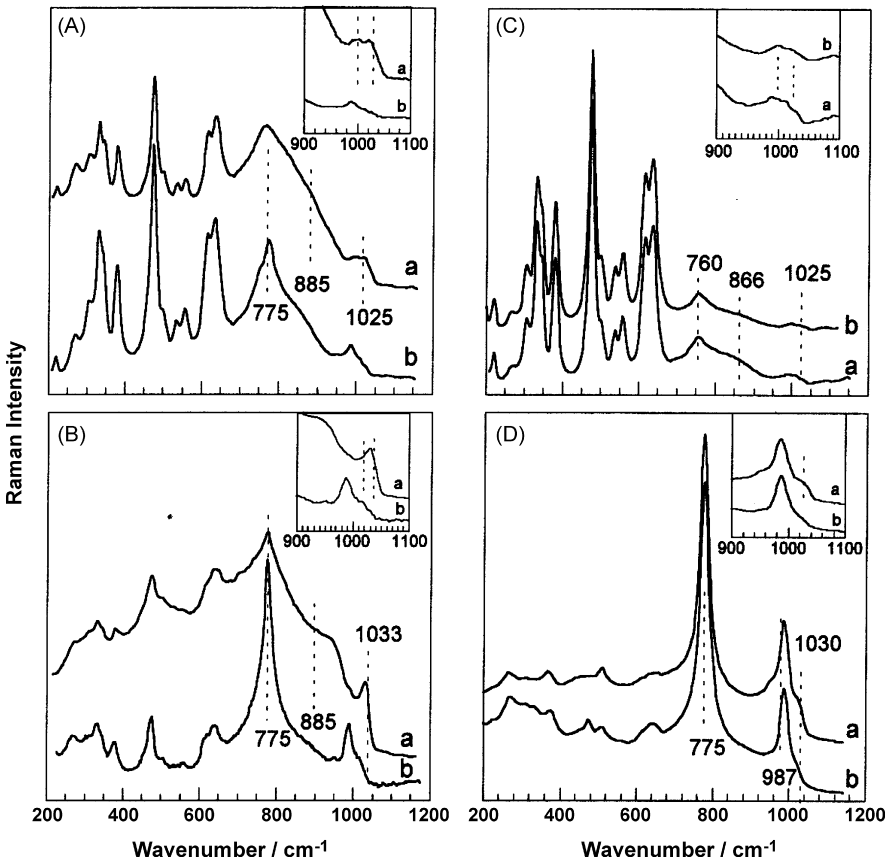

Fig. 3. Raman spectra after *in situ* treatments.
Section A: (a) ZV2.7,10; (b) ZV2.7,10L1.4. Section B: (a) ZV5.4,10; (b) ZV5.4,10L3.0. Section C: (a) ZV1.2,2.7: (b) ZV1.2,2.7L1.1. Section D: (a) ZV7.4,2.7; (b) ZV7.4,2.7L5.8.

as the small polymeric species are reduced faster and at temperatures lower than monovanadate structures ($T < 800$ K) and large polymeric species, the reducibility sequence proposed by Deo and Wachs [54]: V–O–V > V–O–$(V)_2$ > V=O was confirmed. We failed to observe an important peak at 800 K in dilute samples, probably because the monovanadate species, if present, was a minority species. Therefore, in agreement with the Raman conclusion, the TPR data confirm the presence of polymeric vanadium species in our samples. As the concentration increases, the vanadium polymeric structures grow, ZrV_2O_7 forms and the reduction shifts to higher temperature.

The leaching treatment, removing large polymeric species (V_2O_5-like) and V_2O_5 crystallites, yielded simplified TPR profiles for both sets of samples (Fig. 5A–D, curves b). Accordingly, the H_2 consumption decreased in the range 600–800 K and for the ZV11.7,2.7L*z* sample the peak at 900 K ascribed to V_2O_5, disappeared (profile not shown). The broad TPR features centred at 640 K for ZV*x*,10L*z* samples (Fig. 5A and 5B, curves b) and at about 600, 700 and 800 K for ZV*x*,2.7L*z* samples (Fig. 5C and 5D, curves b), originated from the reduction of polymeric species strongly held on the zirconia surface or reacted to form ZrV_2O_7 crystallites or both.

3.2. Catalytic behaviour for the n-butane oxidative dehydrogenation

ZrO_2(823) was inactive. For ZV*x,y* catalysts, neither CO nor butadiene were detected in any experiment. 1-butene was sometimes observed in traces. The C_4H_8 fraction was almost entirely constituted by 2-butenes with *cis/trans* ratio of 0.8–0.85. Thus, hereinafter "C_4H_8" or "butenes" will indicate the sum of *cis* and *trans* 2-butenes. The oxygen conversion values did not exceeded 60%, except in one case (69%, sample ZV3.45,10). The carbon balance generally closed at $100 \pm 3\%$.

The total *n*-butane conversion and the butene selectivity values are collected in Table 2 together with the apparent surface density (total number of V atoms in one gram of catalyst/total surface area of one gram of catalyst) used as a variable for comparison purposes, bearing in mind that it is a functional parameter approaching the exposed V species for dilute samples only to a first approxima-

Table 2
Samples, V surface density (V atoms nm^{-2}) and catalytic properties for *n*-butane oxidative dehydrogenation at 603 K.

Samples[a]	V atoms nm^2	% Total *n*-C_4H_{10} conversion	% Selectivity to C_4H_8
ZV0.99,10	1.5	3.7	63
ZV2.7,10	4.1	9.3	25
ZV3.1,10	3.5	11.6	20
ZV3.4,10	3.2	27.0	44
ZV4.1,10	4.2	21.9	41
ZV6.4,10	6.6	42.3	72
ZV2.7,10L1.4	2.1	5.7	32
ZV4.1,10L2.2	2.2	5.5	34
ZV4.8,10L2.2	2.9	6.3	30
ZV 1.9,2.7	2.9	10.7	40
ZV 2.6,2.7	3.2	10.8	31
ZV3.7,2.7	5.5	24.0	64
ZV 5.9,2.7	18.8	13.8	59
ZV 7.4,2.7	36.5	8.9	60
ZV 7.6,2.7	23.6	14.9	64
ZV 5.9,2.7L2.3	6.5	10.8	52
ZV7.4,2.7L5.8	19.6	5.9	39
ZV7.6,2.7L5.7	15.0	11.6	49

[a] For designation of samples, see text.

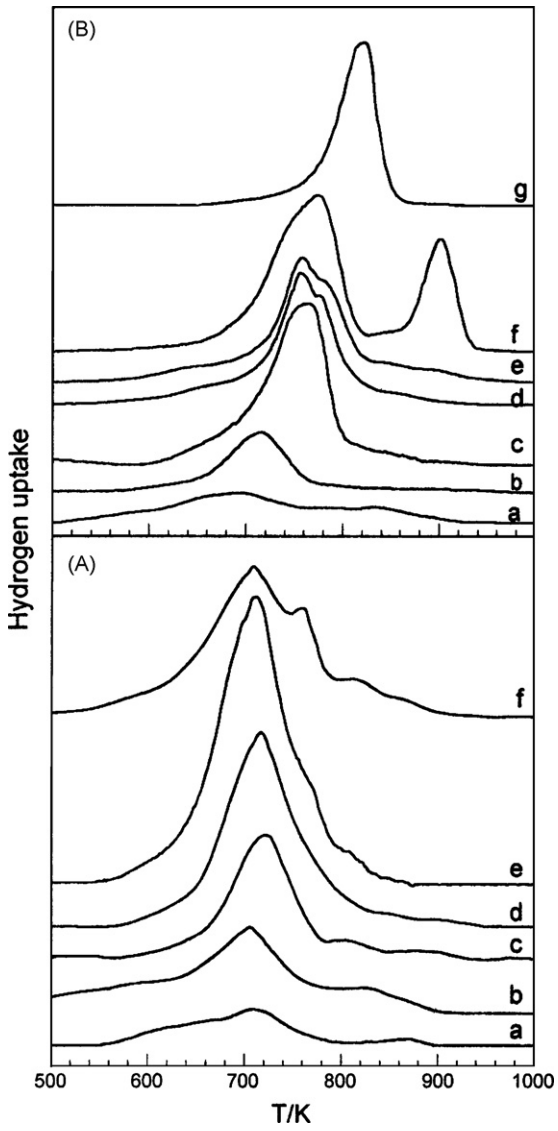

Fig. 4. TPR profile of ZV*x*,10 (A) and ZV*x*,2.7(B) samples.
Section A: (a) ZV0.99,10; (b) ZV2.7,10; (c) ZV3.1,10; (d) ZV3.45; (e) ZV4.25,10; (f) ZV5.4,10. Section B: (a) ZV1.2,2.7; (b) ZV2.6,2.7; (c) ZV5.9,2.7; (d) ZV7.4,2.7; (e) ZV7.6,2.7; (f) ZV11.6,2.7; (g) ZrV_2O_7.

tion. For the ZV*x*,10 and dilute ZV*x*,2.7 samples (V atoms $nm^{-2} < 7$) the areal rate of *n*-C_4H_{10} total conversion, Fig. 6, increased with V loading, reaching the maximum value for an apparent surface density of about 7 V atoms nm^{-2}. For concentrated ZV*x*,2.7 catalysts (V atoms $nm^{-2} > 7$), the areal rate levelled off. Ammonia leaching reduced the areal rate of *n*-C_4H_{10} total conversion for both series of samples.

In vanadia-supported ZrO_2 systems the most active sites for the ODH of propane were associated with polymeric VO_x species [19–21]. These sites were reported to increase with loading and a maximum constant activity was reached, although this occurred at a vanadium density [20] lower than that we found for *n*-butane ODH. The increase in the areal rate of the *n*-C_4H_{10} total conversion with the apparent surface density for the ZV*x*,10 and dilute ZV*x*,2.7 samples (up to 7 V atoms nm^{-2}, $x \leq 3.7$ wt.%), Fig. 6, suggests that the polymeric species are the most active sites also for *n*-butane ODH. As Raman and TPR determinations showed, these samples contain an increasing amount of polymeric material; thus the increasing activity appears correlated with a parallel increase in exposed polymeric species.

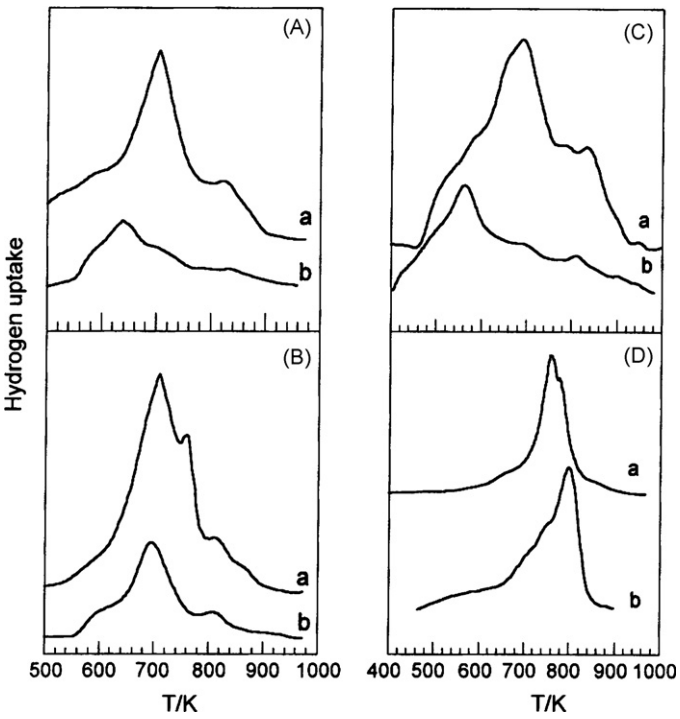

Fig. 5. TPR profiles of some representative ZV*x*,10 samples before and after leaching. Section A: (a) ZV2.7,10; (b) ZV2.7,10L1.4. Section B: (a) ZV5.4,10; (b) ZV5.4,10L3.0. Section C: (a) ZV1.2,2.7; (b) ZV1.2,2.7L1.1. Section D: (a) ZV7.4,2.7; (b) ZV7.4,2.7L5.8.

For concentrated ZV*x*,2.7 catalysts (V atoms $nm^{-2} > 7$), the levelling off of the areal rate may be explained by considering that the increasing loading left the surface density of the exposed vanadium species almost unchanged as the polymeric material increases in thickness over the zirconia particles. This description is in agreement with high resolution electron microscopy findings of Sanati et al. [34] who showed that an amorphous structure of polymeric vanadium material covered the zirconia surface starting from a sample containing 5.3 wt.% of vanadium (apparent surface density = 7.94 V atoms nm^{-2}).

As for pure compounds, no literature data are available for *n*-butane ODH activity of ZrV_2O_7, whereas V_2O_5 reportedly has some

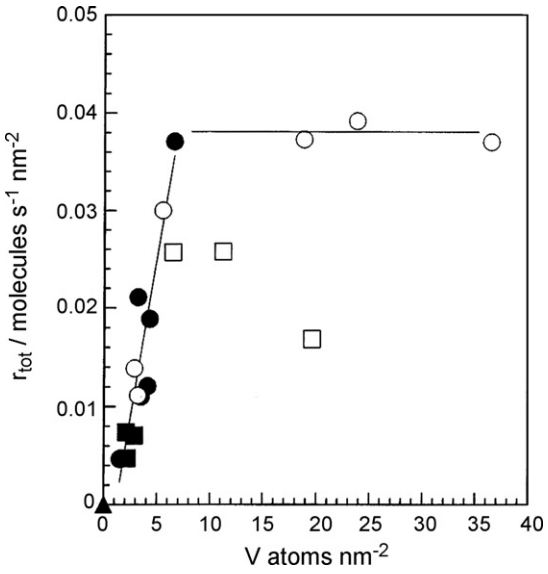

Fig. 6. Areal rate for total *n*-C_4H_{10} conversion at 603 K vs. apparent V surface density: (●) ZV*x*,10; (■) ZV*x*,10L*z*; (○) ZV*x*,2.7; (□) ZV*x*,2.7L*z*; (▲) ZrO_2.

activity for the same reaction [4]. In the present study the contribution of V_2O_5 and ZrV_2O_7 to the samples activity are expected to be low because of their low surface area (as estimated from crystallite-size).

The decrease in the areal rate of the n-C_4H_{10} total conversion we observed for the leached ZV*x*,10L*y* samples (Fig. 6) agrees with the given picture. In fact the leaching removed the active large polymeric aggregates and left ZrV_2O_7 and polymeric species strongly anchored to the support. Similar behaviour is expected for ZV*x*,2.7L*y* samples. For concentrated ZV*x*,2.7Ly samples the apparent surface density remained high owing to the presence of a consistent amount of crystalline ZrV_2O_7.

Although we did not perform a detailed kinetic study and our butene selectivity values refer to different n-C_4H_{10} total conversion, we can note that selectivity data (Table 2) for the concentrated samples from both ZV*x*,10 and ZV*x*,2.7 series are higher than those of the dilute catalysts. Moreover, the leaching decreased both n-C_4H_{10} total conversion and butene selectivity. In a study of the propane ODH reaction, Chen et al. [23] found that the Zr–O–V sites, formed by interaction between vanadium species and support surface, favour alkane combustion. We suggest that the presence of Zr–O–V sites, in the dilute and in the leached samples of both series, could also account for the decreased butene selectivity.

4. Conclusions

Our Raman and TPR data show that at low vanadium content, V < 2.7 wt.%, the structure and spreading of the VO_x species do not depend on the pH (10 or 2.7) adopted for the sample preparation. In both sets of samples the surface species consist mainly of polyvanadate entities. For higher loadings, comparing samples with similar concentration, the fraction of vanadium in a dispersed state and interacting with the support is higher in samples prepared at pH 10 than in those obtained at pH 2.7. In addition, the samples at pH 2.7 contained ZrV_2O_7 and V_2O_5 along with large polymeric species. Leaching with ammonia discloses that small sized polymeric structures interact with the support and ZrV_2O_7 is barely detectable by Raman spectroscopy at low V content on both sets of samples. Relying on the literature findings for propane ODH, we propose that V–O–V bridges could be associated with the active sites for n-butane ODH, whereas the Zr–O–V sites could favour the alkane combustion.

Acknowledgments

Financial support from Italian MIUR (PRIN, Progetti di ricerca di rilevante interesse nazionale) is gratefully acknowledged. The authors thank Mr. Giuseppe Piciacchia for his technical assistance with the Raman Spectrometer.

References

[1] B.M. Weckhuysen, D.E. Keller, Catal. Today 78 (2003) 25–46.
[2] H.H. Kung, Adv. Catal. 40 (1994) 1–35.
[3] F. Cavani, F. Trifirò, Catal. Today 51 (1999) 561–580.
[4] E.A. Memedov, V. Còrtes Corberàn, Appl. Catal. A: Gen. 127 (1995) 1–40.
[5] T. Blasco, J.M.L. Nieto, Appl. Catal. A: Gen. 157 (1997) 117–142.
[6] A.A. Lemonidou, L. Nalbandian, I.A. Vasalos, Catal. Today 61 (2000) 333–341.
[7] G. Centi, Appl. Catal. A: Gen. 147 (1996) 267–298.
[8] F. Cavani, E. Foresti, F. Trifirò, G. Busca, J. Catal. 106 (1987) 251–262.
[9] P. Forzatti, Appl. Catal. A: Gen. 222 (2001) 221–236.
[10] I.E. Wachs, J. Jehng, G. Deo, B.M. Weckhuysen, V.V. Guliants, J.B. Benziger, S. Sundaresan, J. Catal. 170 (1997) 75–88.
[11] J. Haber, in: G. Ertl, H. Knözinger, J. Weitkamp (Eds.), Handbook of Heterogeneous Catalysis, vol. 5, Wiley VCH, Weinheim, 1997, pp. 2253–2274.
[12] M.D. Argyle, K. Chen, A.T. Bell, E. Iglesia, J. Catal. 208 (2002) 139–149.
[13] V. Bràzdová, M.V. Ganduglia-Pirovano, J. Sauer, J. Phys. Chem. B 109 (2005) 23532–23542.
[14] M. Olea, I. Sack, V. Balcaen, G.B. Marin, H. Poelman, K. Eufinger, D. Poelman, R. De Gryse, J.S. Paul, B.F. Sels, P.A. Jacobs, Appl. Catal. A: Gen. 318 (2007) 37–44.
[15] F. Klose, T. Wolff, H. Lorenz, A. Seidel-Morgenstern, Y. Suchorski, M. Piórkowska, H. Weiss, J. Catal. 247 (2007) 176–193.
[16] C.L. Pieck, M.A. Bañares, J.L.G. Fierro, J. Catal. 224 (2004) 1–7.
[17] H. Poelman, B.F. Sels, M. Olea, K. Eufinger, J.S. Paul, B. Moens, I. Sack, V. Balcaen, F. Bertinchamps, E.M. Gaigneaux, P.A. Jacobs, G.B. Marinc, D. Poelmana, R. De Grysea, J. Catal. 245 (2007) 156–172.
[18] M. De, D. Kunzru, Catal. Lett. 96 (2004) 33–42.
[19] A. Khodakov, J. Yang, S. Su, A.T. Bell, E. Iglesia, J. Catal. 177 (1998) 343–351.
[20] J.L. Male, H.G. Niessen, A.T. Bell, T. Don Tilley, J. Catal. 194 (2000) 431–444.
[21] A. Khodakov, B. Olthof, A.T. Bell, E. Iglesia, J. Catal. 181 (1999) 205–216.
[22] K. Chen, A. Khodakov, J. Yang, A.T. Bell, E. Iglesia, J. Catal. 186 (1999) 325–333.
[23] K. Chen, A.T. Bell, E. Iglesia, J. Phys. Chem. B 104 (2000) 1292–1299.
[24] A. Dinse, B. Frank, C. Hess, D. Habel, R. Schomäcker, J. Mol. Catal. A: Chem. 289 (2008) 28–37.
[25] J.M. López Nieto, P. Concepción, A. Dejoz, F. Meloa, H. Knözinger, M.I. Vázquez, Catal. Today 61 (2000) 361–367.
[26] L.M. Madeira, M.F. Portela, Catal. Rev. Sci. Eng. 44 (2002) 247–286.
[27] M.A. Bañares, I.E. Wachs, J. Raman Spectrosc. 33 (2002) 359–380.
[28] O. Ovsitser, E.V. Kondratenko, Catal. Today 142 (2009) 138–142.
[29] M. Valigi, D. Gazzoli, G. Ferraris, S. De Rossi, R. Spinicci, J. Mol. Catal. A: Chem. 227 (2005) 59–66.
[30] J.Ph. Nogier, Catal. Today 20 (1994) 23–34.
[31] G. Centi, E. Giamello, D. Pinelli, F. Trifirò, J. Catal. 130 (1991) 220–237.
[32] B. Grzybowaska-Świerkosz, Appl. Catal. A: Gen. 157 (1997) 263–310.
[33] A. Cimino, S. De Rossi, R. Dragone, G. Ferraris, D. Gazzoli, M. Valigi, J. Colloid. Interface Sci. 201 (1998) 278–292.
[34] M. Sanati, A. Andersson, L.R. Wallenberg, B. Rebenstorf, Appl. Catal. A: Gen. 106 (1993) 51–72.
[35] R.C. Weast, M.J. Astle (Eds.), C. R. C. Handbook of Chemistry and Physics, 63rd ed., C.R.C. Press, Inc., Boca Raton, Florida, 1982, p. B–162.
[36] Powder Diffraction File, JCPDS-International Center for Diffraction Data Swarthmore, Pennsylvania, 1991. File 41-1426.
[37] Powder Diffraction File, JCPDS-International Center for Diffraction Data Swarthmore, Pennsylvania, 1991. File 16-422.
[38] P.E. Thomas, W.F. Pickering, Talanta 18 (1971) 127–137.
[39] I. Pettiti, D. Gazzoli, M. Inversi, M. Valigi, S. De Rossi, G. Ferraris, P. Porta, S. Colonna, J. Synch. Rad. 6 (1999) 1120–1124.
[40] K. Chen, S. Xie, E. Iglesia, A.T. Bell, J. Catal. 189 (2000) 421–430.
[41] M. Valigi, D. Gazzoli, I. Pettiti, G. Mattei, S. Colonna, S. De Rossi, G. Ferraris, Appl. Catal. A: Gen. 231 (2002) 159–172.
[42] X. Gao, I.E. Wachs, J. Phys. Chem. B. 104 (2000) 1261–1268.
[43] X. Gao, J. Jehng, I.E. Wachs, J. Catal. 209 (2002) 43–50.
[44] A. Christodoulakis, M. Machli, A.A. Lemonidou, S. Boghosian, J. Catal. 222 (2004) 293–306.
[45] D.E. Keller, D.C. Koningberger, B.M. Weckuysen, J. Phys. Chem. B 110 (2006) 14313–14325.
[46] C.V. Ramana, R.J. Smith, O.M. Hussain, M. Massot, C.M. Julien, Surf. Interface Anal. 37 (2005) 406–411.
[47] I.E. Wachs, Catal. Today 27 (1996) 437–455.
[48] D. Gazzoli, G. Ferraris, S. De Rossi, M. Valigi, L. Ferrari, S. Selci, Appl. Surf. Sci. 255 (2008) 2012–2019.
[49] H. Bosch, B.J. Kip, J.G. van Ommen, P.J. Cellings, J. Chem. Soc., Faraday Trans. 1 (80) (1984) 2479–2488.
[50] G.C. Bond, S. Tair, Appl. Catal. A: Gen. 71 (1991) 1–31.
[51] J. Pieck, S. del Val, M.L. Granados, M.A. Bañares, J.L.G. Fierro, Langmuir 18 (2002) 2642–2648.
[52] F. Roozeboom, M.C. Mittelmeijer-Hazeleger, J.A. Moulijn, J. Medema, V.H.J. de Beer, P.J. Gellings, J. Phys. Chem. 84 (1980) 2783–2791.
[53] A. Adamski, Z. Sojka, K. Dyrek, M. Che, G. Wendt, S. Albrecht, Langmuir 15 (1999) 5733–5741.
[54] G. Deo, I.E. Wachs, J. Catal. 129 (1991) 307–312.